ORIGINAL PAPER

Investigating the Roles of Protein on the Cobalt Alloy Surface Degradation for Biomedical Implant Through Tribocorrosion Mechanisms

Mohamad Taufiqurrakhman[1,3] · Thawhid Khan[1] · Michael G. Bryant[2]

Abstract
Previous investigation has established the formation of tribofilm is influenced by tribochemical reactions between the electrolyte and the articulating surface of cobalt alloy through sliding tests in various simulated fluids. Although it has successfully characterized the film composition via spectroscopy analysis and indicated to have impact on material loss, a comprehensive understanding of the material degradation mechanism in tribocorrosion condition was still lacking. Therefore, this study aims to investigate the role of protein in the tribocorrosive degradation of cobalt-chromium-molybdenum (CoCrMo) alloy in different simulated physiological electrolytes. Using a similar testing protocol, tribocorrosion tests were conducted with reciprocating ceramic ball against CoCrMo samples immersed in saline and culture medium, compared to both electrolytes diluted with 25% fetal bovine serum (FBS). Synergistic and mechanistic approaches were employed to model the tribocorrosive degradation. Results reveal that protein plays a beneficial role in reducing corrosive (electrochemical) surface degradation under tribocorrosion condition, whilst increasing mechanical wear degradation in the process. Despite studies have shown that tribocorrosion behavior in metal alloys is highly influenced by the presence of organic matter, this study provides a more clarity of the roles played by protein in tribocorrosive degradation on CoCrMo surface as its novel finding.

Keywords Serum protein · CoCrMo alloy · Tribocorrosion · Synergistic · Hip implant

1 Introduction

CoCrMo is a widely used bearing material in hip and knee arthroplasties due to its mechanical properties, self-mating performance, and perceived biocompatibility [1–3]. However, concerns have arisen about the release of metal ions and debris into the biological environment, questioning its suitability for biomedical applications [4–8]. Tribocorrosion process is a primary contributor to the simultaneous generation of metallic debris (mechanical wear) and ion release (electrochemical corrosion) on articulating components [9–11]. To achieve reduced wear and corrosion, a thorough understanding of the fundamental surface degradation mechanisms is essential [12]. It is important to note that tribocorrosion cannot be simplified to the straightforward addition of wear and corrosion losses, given its simultaneous mechanical and chemical events [9, 13–15]. Additionally, comprehending the interactions between contacting surfaces and biological fluid is crucial in determining the tribocorrosive degradation of implant materials. Therefore, effective control of tribocorrosion requires a distinct strategy.

Tribocorrosion can be effectively studied using the synergistic approach [6–9]. A standardized method (ASTM G119) has been proposed, considering the combined effects of mechanical wear and electrochemical corrosion, along with a synergistic factor involving wear-induced corrosion and corrosion-induced wear [16]. That standard has been widely used in various studies [14, 17–22] to quantify the synergism of different materials in diverse environments, which can be categorized as antagonistic or synergistic [2, 23]. In response to certain limitations of the synergistic

✉ Mohamad Taufiqurrakhman
 menmtau@leeds.ac.uk

1 Institute of Functional Surfaces (iFS), School of Mechanical Engineering, University of Leeds, Leeds LS2 9JT, UK

2 Department of Mechanical Engineering, School of Engineering, University of Birmingham, Birmingham, B15 2TT, UK

3 Present Address: Leeds Institute of Rheumatic and Musculoskeletal Medicine (LIRMM), School of Medicine, University of Leeds, Leeds LS9 7TF, UK

approach, the mechanistic approach initially developed by Uhlig [24], was standardized as UNE 112086 [25]. This mechanistic approach identifies two primary mechanisms governing tribocorrosion: mechanical removal due to wear and anodic dissolution/corrosion during intermittent depassivation. However, the approach was later refined to account for additional factors, such as pure passive corrosion beyond the contact area and corrosion-enhanced wear loss [26]. The mechanistic approach has gained popularity among researchers due to its simplicity and effectiveness [27–31]. Understanding these interactions is vital in assessing the performance of materials under tribocorrosion conditions with the biological species presence, such as protein, in the physiological environment as the complexity factors.

Proteins are the predominant molecule in synovial fluid, which exhibit a complex structure of amino acids and is stabilized by various interactions [32, 33]. Studies have demonstrated some effects of the protein when interacting with metal surface, such as on metal-oxide bonding, surface film, corrosion reactions, and tribocorrosion properties [27, 34–41]. While Munoz and Mischler [27, 35, 36] investigated that protein adsorption increases the corrosion rate of CoCrMo alloy [27, 35, 36], Yan et al. [42, 43] presented that it significantly enhances the corrosion resistance of articulating metal surface as also appeared in several other studies [44, 45]. This shows the protein can act multiple roles depending on its operating environment. The protein molecule reactivity toward the surface is affected by the electrochemical potential and tribological conditions [35, 46, 47]. Interestingly, studies hypothesized that protein contributed to abrasive wear, even though it tended to deposit as a film on the metal surface during sliding [29, 48, 49]. When protein possesses unfolded structures due to shear stress or increased temperature, it can easily complex with the metal or aggregate with other protein, forming protein-metal complexes that act as abrasive particles, accelerating material degradation rates. These protein particles can also lead to the increased friction, material wear, and inflammatory oxidative conditions [50].

This study was done as a follow-up investigation based on the previous findings published by the authors [11], which successfully characterized the structure of tribofilms deposited in the wear scar on CoCrMo surfaces. It was noted from the previous study, the proteinaceous species such as calcium, phosphorus, and sulfur were catalyzed by tribology-induced processes, leading to their deposition onto the tribofilm, as confirmed by the X-ray photoelectron spectroscopy (XPS) profiling analysis. Moreover, the addition of protein in simulated physiological fluids was indicated to enhance corrosion resistance. The average coefficients of friction (μ) observed during 2 h of sliding over CoCrMo–alumina interfaces were found to be significantly lower in electrolytes that contained organic species,

including protein and cell culture medium when compared to the μ measured in saline solutions, in which the reduction in μ was more than 50%. This observation suggested that the presence of organic substances had a substantial lubricating effect during the sliding process, resulting in lower friction. However, a comprehensive understanding of the material degradation process in the presence of protein during tribocorrosion remains largely unknown.

There are only a limited number of recent studies investigating tribocorrosion behavior in cobalt alloys with the presence of organic matter in the testing environment, employing both mechanistic and synergistic approaches to understand material mass loss mechanisms. Therefore, this study aims to explore the role of protein substances in the tribocorrosive degradation mechanism of CoCrMo alloy surfaces using both tribocorrosion approaches. As a novel finding, this investigation reveals that protein plays a "double agent" role during tribocorrosion tests. On one hand, its presence reduces corrosive (electrochemical) surface degradation, yet on the other hand, it tends to elevate mechanical wear degradation during sliding tests when compared to tests conducted without protein. This study is expected to highlight on the protein–metal surface interaction under tribocorrosion, contributing to a broader understanding of their performance in physiological environments in order to later design of new materials in orthopedic implant applications.

2 Material and Methodology

Figure 1 shows a schematic of the overall experimental procedures employed in this study, including the list of testing electrolytes, tribocorrosion testing methods, surface analysis, and measurements to obtain tribocorrosive degradation components and then analyzed by tribocorrosion approaches.

2.1 Testing Materials

The testing materials employed in this study consisted of CoCrMo samples immersed in four different electrolytes. The CoCrMo alloy used in this study was a wrought low-carbon Co-28Cr-6Mo alloy, complying with ASTM F75-12 standard specifications [51]. The 22-mm diameter rod supplied by Peter Brehm GmbH, Germany, was cut into flat components of 6 mm thickness. The samples were prepared by grinding with silicon carbide paper (grit sizes 600–1200) followed by mirror-polishing using 3 and ¼ μm diamond paste and polishing paper (Bruker Corporations, UK) to achieve an approximate surface Ra of ~5 nm. After degreasing with acetone, rinsing with deionized (DI) water, and drying with compressed air, the CoCrMo samples were

Fig. 1 Schematic of tribocorrosion tests, surface analysis protocols, and components to achieve tribocorrosion approaches
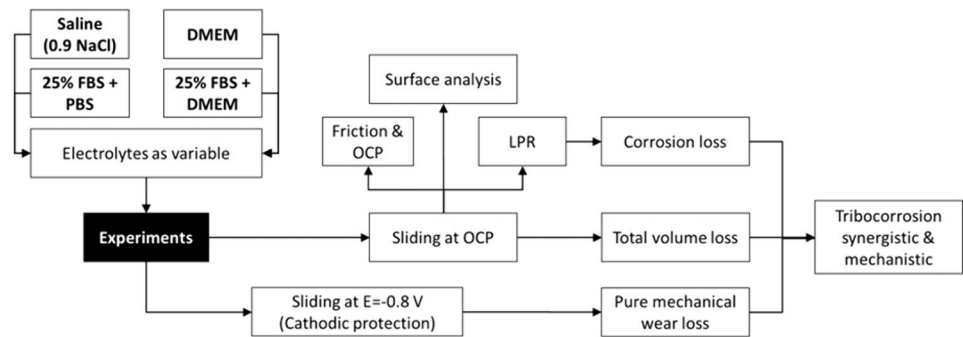
used directly for tribocorrosion testing. This preparation method aligns with practices within the field [52–55] and complies with ASTM G5 [56] and G59 [57] guidance.

This study compared four different electrolytes used as seen in Table 1, as also detailed in the previous study [11]. Analytical laboratory-grade sodium chloride (NaCl) from Sigma, UK, was used as the received salt ion in this study. The pure saline consisted of 0.9% w/v sodium chloride (NaCl) in deionized water with a viscosity of 0.000885 Pa.s [58] as one of the electrolytes. One of the organic-containing electrolytes, devoid of protein, lipids, or growth factors, was a high-glucose Dulbecco's modified Eagle's medium (Gibco's DMEM) solution from Life Technologies Corporation, UK. This solution contained Mg ions from magnesium sulfate ($MgSO_4$–$7H_2O$). The DMEM had a high-glucose level of 4.5 mg/mL, along with a substantial concentration of amino acids, vitamins, and inorganic salts. With a pH of 7.2 and conductivity of 0.68 mS/cm, this solution was commonly used in cell culture processing applications. DMEM possessed the same chloride content as FBS, which influenced the corrosion behavior [59–61].

Fetal bovine serum (FBS) from Sera Laboratories International, UK, was used as the testing electrolyte, filtered at triple 0.1 μM and European grade. The FBS concentration was in accordance with the version of ISO 14243-3 standard for hip simulation, necessitating a 25% (v/v) concentration of serum or a minimum 17-g/L total protein content [61–63]. For this study, the 25% FBS was diluted in phosphate-buffered saline (PBS) and the DMEM solution to investigate the effect of protein in the physiological

electrolyte composition as comparison to the as-received saline and DMEM solutions.

2.2 Tribocorrosion Tests

A reciprocating tribometer (BICERI, UK) was utilized to simulate tribocorrosion, employing a reciprocating alumina (Al_2O_3) ceramic ball with a diameter of $\emptyset = 12$ mm and grading standard of 25 (Atlas Ball and Bearing Company, UK). The ceramic ball was in direct contact with a flat CoCrMo sample, exposing an area of 3.80 cm². To achieve an initial mean Hertzian contact pressure (P_{mean}) of 815 MPa, a constant normal load of 30 N was applied [11, 64]. The applied contact pressure aimed to simulate an extreme movement of the hip joint, exceeding that of normal standard gait condition [11, 29, 61].

All tests were conducted with a 10-mm stroke length, 1-Hz frequency, and sliding speed of 20 mm/s (1 cycle per second in tribocorrosion test) at room temperature (~ 25 °C) under equilibrium conditions (i.e., corrosion not forced). The total sliding time was 2 h, and each test was conducted in triplicate ($n = 3$). After the tests, the samples underwent a rapid rinse with DI water, were dried with compressed air, and then stored in a desiccator to prevent contamination before surface chemical analysis.

The reciprocating pin-on-plate tribometer was equipped with a 3-electrode electrochemical cell controlled via a PGSTAT101 potentiostat (Metrohm Autolab, the Netherlands), as depicted in Fig. 2 (reproduced from the previous study [11, 29]). The electrochemical cell consisted of the CoCrMo sample as the working electrode (WE), a silver/

Table 1 Characteristics of the testing electrolytes [11]

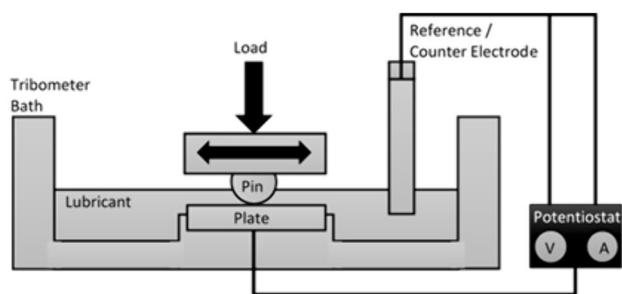| Electrolytes	pH	Conductivity (mS/cm)	Viscosity (mPa s)	Lambda ratio λ	Protein (gram per volume)
Saline	6.9	3.8	0.88	0.019	0 g/L
25% FBS + PBS	7.4	3.8	< 1	0.021	17 g/L
DMEM	7.2	0.68	1.07	0.022	0 g/L
25% FBS + DMEM	7.2	0.68	1.07	0.022	17 g/L

Fig. 2 Instrumented reciprocating tribometer scheme (image was reproduced from the previous study [11])

silver chloride (Ag/AgCl) as the reference electrode (RE), and a platinum (Pt) disk as counter electrode (CE).

2.2.1 Electrochemical Measurements

Corrosion and tribocorrosion were assessed using open-circuit potential (OCP) and intermittent linear polarization resistance (LPR) measurements, consistent with the approach used in the previous studies [11, 29]. OCP was determined by recording the potential difference between the working electrode (WE) and reference electrode (RE) at a rate of 1 Hz. The absence of current flow between the counter electrode (CE) and WE indicated equilibrium between the anodic and cathodic reactions of the CoCrMo sample. Monitoring the OCP evolution during the test provided a semi-quantitative evaluation of the system's corrosion behavior. A previous study [65] apparently have done critiques on the LPR measurement, in which it has benefit as it can calculate a wide range of corrosion resistance with a straightforward method. By applying relatively small over-potential and determining the ratio of voltage over current through the three electrodes in an electrolyte, the corrosion parameters can be monitored and calculated, without additional data processing and destructing the sample [66, 67]. To note that in some cases it may be difficult to measure accurately the corrosion resistance when the environment containing the electrode does not form a linearity between over-potential and current density, as well as has limitations when measured in severe corrosive circumstances [68, 69].

Intermittent LPR measurements were conducted at 500 s after immersion, followed by 30-min intervals during sliding

and finally at 500 s after the test to assess the material's resistance to polarization and subsequent corrosion current. To calculate the polarization resistance (R_p), the potential of the WE were shifted ± 10 mV versus OCP with a scan rate of 0.25 mV/s, and the resulting current was measured. The LPR technique, operating within a few millivolts (mV) of the sample OCP, is considered non-destructive. Conducting LPR measurements intermittently avoided potential changes within the system that might arise from sustained over-potential application. ASTM G119-09 [70] and G59-97 [57] outline the use of the LPR technique and Stern–Geary coefficients to determine corrosion currents in tribocorrosion systems [60]. Figure 3 provides an overall schematic of the tribocorrosion tests in OCP conditions.

Figure 4 presents example plots of current versus potential obtained from LPR tests under (a) static and (b) sliding conditions (example tested in saline) [29]. A linear E–I response was observed around zero net current. The slope of the measured current as a function of applied potential represents the polarization resistance, calculated using a voltage window of ± 5 mV around zero net current, consistent with previous studies [11, 29, 71]. The R_p values were then converted into corrosion current density (I_corr) in Amperes using the Stern–Geary formula (Eq. 1) and standard Tafel constants (β_a and $\beta_\text{c} = 120$ mV/decade) obtained through extrapolation of the Tafel plot. In this study, the values of both R_p and I_corr were plotted and obtained by CorrWare and CorrView software (AMETEK Scientific Instruments, USA). The obtained I_corr values were integrated over the tribocorrosion test time (t) in seconds to determine the total charge transfer of ion removal (Q) in Coulombs, as described in Fig. 4c and Eq. (2) [71].

$$I_\text{corr} = \frac{\beta_\text{a} \cdot \beta_\text{c}}{2.303 \left(\beta_\text{a} + \beta_\text{c} \right)} \cdot \frac{1}{R_\text{p}}, \tag{1}$$

$$Q = \int_0^t I_\text{corr} dt. \tag{2}$$

The charge transfer obtained from LPR data was used to estimate the mass loss (m) of the metallic surface resulting from corrosion components, following Faraday's Law (Eq. 3). Faraday's constant (F) of 96,500 C/mol and the molar mass (M) of 55.7 g/mol, obtained from the

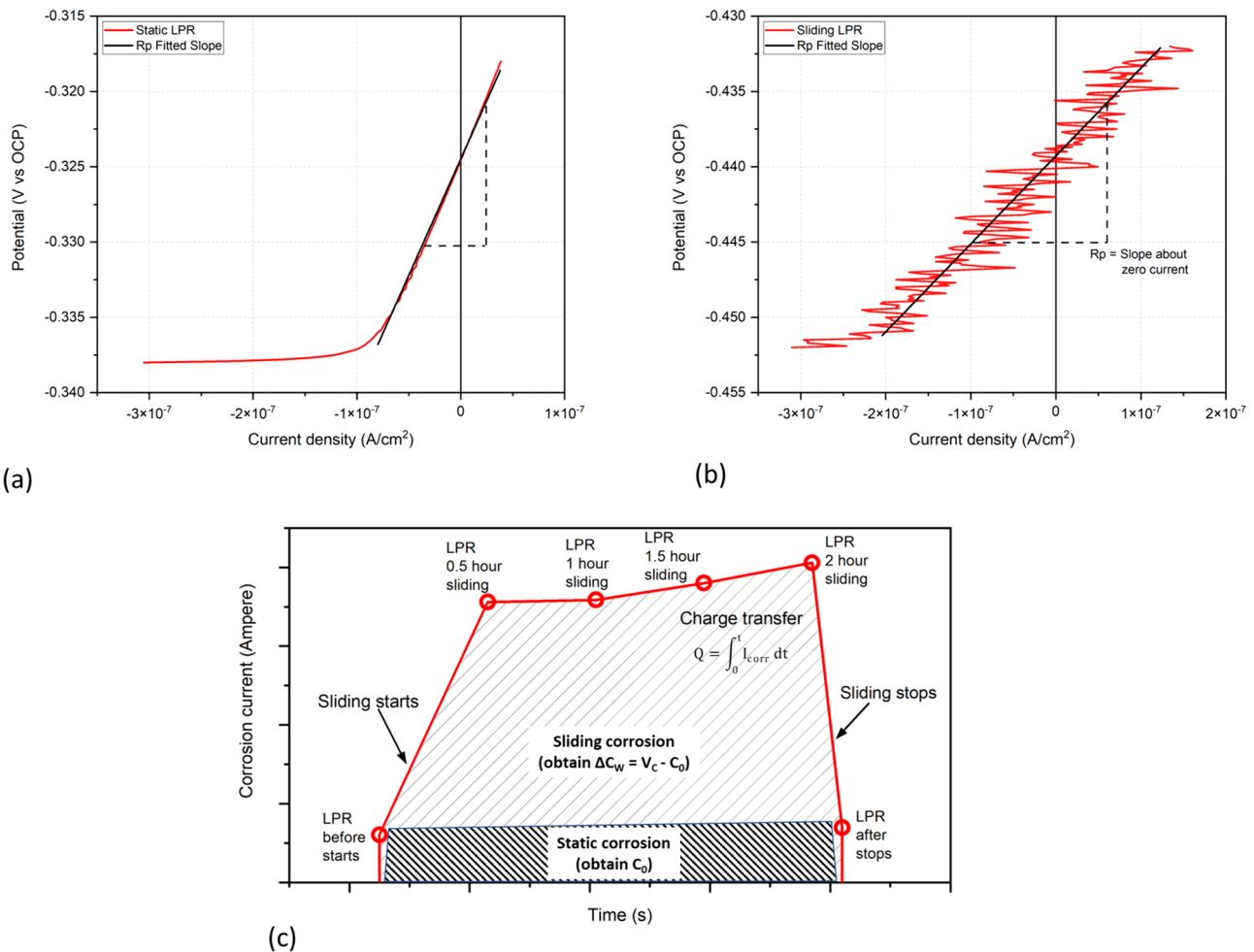**Fig. 3** Schematic of the tribo-corrosion tests' procedure in OCP condition
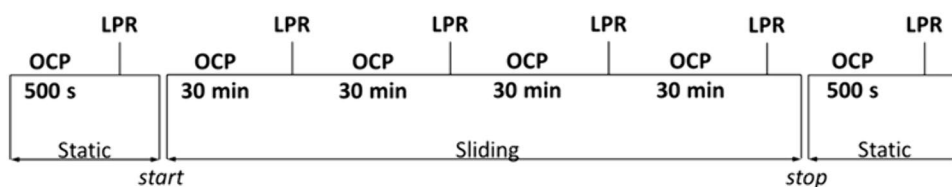
Fig. 4 Example of polarizations during LPR scan at **a** static and **b** sliding conditions in 0.9% NaCl, as well as **c** plotted I_{corr} values over testing time to obtain the total charge transfer

stoichiometric average of CoCrMo alloys composition, yielded a valence number (n) of 2.4 and a density (ρ) of 8.29 g/cm^3. These values were consistent with those used in previous studies involving CoCrMo samples [11, 29, 71–73]. The estimated mass loss was then divided by the material density to calculate the corrosion volume loss (V_C) in accordance with Eq. (4).

$$M = \frac{M.Q}{n.F}, \tag{3}$$

$$V_C = \frac{m}{\rho}. \tag{4}$$

2.2.2 Cathodic Potentiostatic Polarization

Potentiostatic polarization was employed to monitor the transient cathodic net current behavior at a fixed (static) potential between the working electrode (WE) and reference electrode (RE). Applying a fixed cathodic potential was intended to inhibit the oxidation of the metal surface. By applying cathodic potential during sliding, corrosion damage could be avoided, allowing for the measurement of pure mechanical wear loss (W_0) at the surface. Friction coefficient data were not shown for this test. Prior to potentiostatic testing, samples ($n = 3$) were immersed in OCP to stabilize surface passivation for 500 s. Subsequently, a constant potential was applied ($E = -0.8$ V in this study) and the tribological condition was introduced at 60 s after potentiostatic condition started. The potentiostatic tests were conducted under sliding conditions for a duration of 2 h. After finished, the cleaning procedure was conducted for CoCrMo samples as similar as the ones in OCP condition and then the samples were moved for the volume loss measurements.

2.3 Surface Analysis

Vertical scanning interferometry (VSI) (NPFlex, Bruker, USA) was utilized to acquire three-dimensional surface profiles and measure the total volume loss after 2-h sliding. VSI utilized white light and surface reflection to generate fringes, employing a 10× magnification lens. The Vision64 software (Bruker, MA, USA) processed the results, calculating the wear scar contour and negative volume after removing surface form and tilts. To measure the total volume loss, the layer height was adjusted to calculate all points below the plane.

Specific wear rates were then determined using Archard's Law [74, 75]. As shown in Eq. (5) [76], the specific wear rate (SWR) in μm^3/N.m was calculated by dividing the total volume loss (V_{total}) in μm^3 by the constant normal load (W) in Newton and the sliding run distance (ΔS) of 144 m for the 2-h sliding duration. In this study, VSI measured surface losses from CoCrMo samples under (i) OCP condition to obtain the total volume loss (V_{total}) in μm^3 for a tribocorrosion system at equilibrium and (ii) cathodic potentiostatic to obtain the pure mechanical wear losses (W_0) in μm^3 comparing various electrolytes.

A Carl Zeiss' EVO MA 15 scanning electron microscopy (SEM) was employed to examine the worn surface morphology and particle depositions on the sample surface. The images captured are expected to qualitatively support the findings from the volume losses calculation.

$$V = SWR.W.\Delta S. \tag{5}$$

2.4 Tribocorrosion Analysis

This study used both synergistic and mechanistic approaches to analyze the tribocorrosive behavior under the given testing conditions, aimed to fill the gap left by the previous study [11].

2.4.1 Synergistic Mode

In this study, the ASTM G119 standard [77] was employed to determine the material loss of the CoCrMo samples following the tribocorrosion test. This standard encompasses four contributing factors: pure mechanical wear (W_0), pure corrosion (C_0), and the combined effects of wear and corrosion (S), as described by Watson's formula in Eq. (6) [9]. The S components can be further divided into two parts: the increase in wear loss due to corrosion dissolution (corrosion-enhanced wear; ΔW_c)

and the increase in corrosion loss due to mechanical wear (wear-enhanced corrosion; ΔC_w).

$$
\begin{aligned}
V_{total} &= W_0 + C_0 + S \\
V_{total} &= W_0 + C_0 + (\Delta W_c + \Delta C_w)
\end{aligned} \tag{6}
$$

In summary, all material loss contributors were converted into 'volume loss' (μm^3) based on the standard procedure. V_{total} was measured using VSI during the tribocorrosion test at OCP condition, representing the cumulative material loss. The C_0 and ΔC_w were estimated from the corrosion current measured by LPR scans during static immersion and the tribocorrosion sliding test, respectively, using Faraday's Law to convert electrochemical currents into volume loss. The W_0 was determined by VSI after the potentiostatic sliding test at the cathodic potential of -0.8 V. Finally, ΔW_c was estimated by subtracting the V_{total} from the combined contributions of W_0, C_0, and ΔC_w. The role of electrolytes was expected to be revealed clearer from this result on the tribocorrosive degradation.

The synergistic behavior of corrosion and wear was evaluated by the ratio between corrosion-enhanced wear (ΔW_c) and wear-enhanced corrosion (ΔC_w). These interactions were categorized as antagonistic, antagonistic-synergistic and synergistic [23], as follows:

- Antagonistic: $\Delta W_c / \Delta C_w < 0.1$
- Antagonistic-synergistic: $1 > \Delta W_c / \Delta C_w \geq 0.1$
- Synergistic: $\Delta W_c / \Delta C_w > 1$

2.4.2 Mechanistic Mode

To complement the synergistic approach, the mechanistic approach by Uhlig's formula in Eq. (7) [24] was employed to estimate the dominant degradation mechanism in the various electrolytes. Based on previous studies by Stack et al. [28, 78], the total volume loss (V_{total}) was divided into two components: corrosion volume loss (V_C) and mechanical wear volume loss (V_W).

$$
\begin{aligned}
V_{total} &= V_W + V_C \\
V_C &= C_0 + \Delta C_w \text{ and } V_W = W_0 + \Delta W_c
\end{aligned} \tag{7}
$$

The ratios between V_C over V_W were then used to determine the specific tribocorrosion mechanisms [28, 78]. The following criteria were applied to identify the dominant tribocorrosion mechanisms:

- Wear: $V_C / V_W \leq 0.1$
- Wear-corrosion: $0.1 < V_C / V_W \leq 1$
- Corrosion-wear: $1 < V_C / V_W \leq 10$
- Corrosion: $V_C / V_W > 10$

2.5 Statistical Analysis

The results are presented as averages with error bars representing the standard deviation (SD). Statistical analysis was performed using one-way analysis of variance (ANOVA). The tested samples (n) were grouped based on testing electrolytes for comparison. ANOVA was employed to determine the significance of the electrolyte's effect on the tribocorrosive degradation of the CoCrMo surface. A significance level of $\alpha = 0.05$ was used, and the p-value was compared in the mentioned comparison. Results with a p-value less than 0.05 were considered significantly different and indicated by an asterisk (*).

3 Results

3.1 Friction and OCP

Figure 5a and b show the transient trend of μ and OCP voltages per sliding cycle, respectively. Both μ and OCP voltages were recorded simultaneously during the tribocorrosion sliding tests, with three repetitions, but the figures visualize one result for each electrolyte. It was evident that the μ in saline was consistently the highest from the beginning of the sliding test compared to organic-containing electrolytes. It started below $\mu \sim 0.35$ and gradually increased over cycles, stabilizing at around $\mu \sim 0.37 \pm 0.03$ after 5,000 cycles. In DMEM, μ started at the lowest value of 0.10 and gradually increased to 0.14 at 1,800 cycles. It was stable, then after 5,200 cycles, the μ tended to gradually increase reaching more than 0.16 ± 0.02 at the end of the test. However, there was a possibility of an increasing μ if the test continued with more cycles. Conversely, protein-containing electrolytes (25% FBS + PBS and 25% FBS + DMEM) showed a higher μ at the starting point (~ 0.15 and 0.13, respectively) compared to the DMEM sample. However, both electrolytes showed mixed of gradual decreases and steady states in μ after 2,000 cycles, reaching 0.13 ± 0.01 and 0.12 ± 0.02 for 25% FBS + PBS and 25% FBS + DMEM, respectively, at the end of the tests, which was significantly lower than that observed in pure DMEM. Interestingly, most of the transient data of μ had a change of trend when closely to 2,000 cycles of sliding test.

Regarding open-circuit potential (OCP), in the pre-sliding stage, CoCrMo in saline exhibited the highest (more noble)

Fig. 5 The evolution of the transient **a** μ and **b** OCP voltages over 2-h sliding cycles under OCP conditions
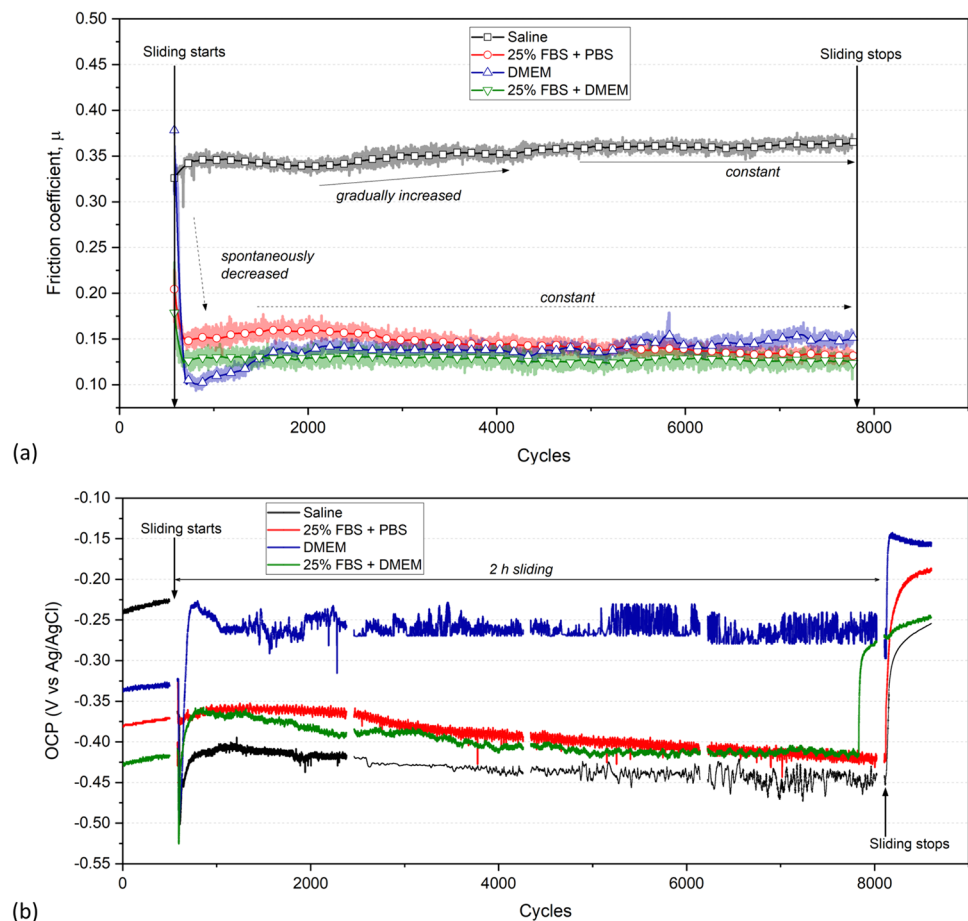
OCP at above -0.25 V followed by DMEM and both 25% FBS-containing electrolytes, which had less than -0.33 V. When sliding started, all samples had a spontaneous reduction in the OCP voltages due to the de-passivation process and then followed by the gradual increase until reaching some points on the voltages due to re-passivation. Interestingly, different electrolytes showed various trends; the sliding OCP in saline were still significantly lower than the pre-sliding condition at -0.40 V at start with slightly decreased until the end of sliding. The sliding OCP in 25% FBS + PBS were seen to be recovered back to the state, whereas like the pre-sliding voltages, at around -0.36 V with gradual decreased until the sliding stopped. In the contrary, DMEM and 25% FBS + DMEM showed higher sliding OCP voltages compared to the trends during pre-sliding. However, the samples in 25% FBS + DMEM (-0.36 V) had similar trend with the 25% FBS + PBS sample, in which did not show re-passivation OCP as significant as in the pure DMEM solution (-0.26 V) during sliding. After the sliding stopped, OCP voltages in all electrolytes had a spontaneous increase reaching points even significantly higher (more noble) compared to the pre-sliding voltages.

3.2 Electrochemical Loss

Table 2 presents the average I_{corr} values through LPR measurements during both static and sliding test conditions. The plotted I_{corr} values against time were represented in the style of Fig. 4c, which has been visualized in the previous study [11]. The I_{corr} values after 500 s of the samples immersion in saline was the highest, followed by DMEM samples. These two electrolytes had significantly higher I_{corr} values compared to the 25% FBS + PBS and 25% FBS + DMEM samples. A similar trend was seen during the sliding condition, with the I_{corr} values in saline were always the highest

reaching 4.42 ± 0.93 μA.cm^{-2} after 4,260 cycles. The I_{corr} values in DMEM samples at sliding were seen to be significantly lower than the saline, however, higher compared to both 25% FBS-containing electrolytes. It seems that the 25% FBS + DMEM results overall were significantly lower than DMEM due to the FBS dilution. No statistical difference was found in the results between 25% FBS + PBS and 25% FBS + DMEM. After 500 s following to the sliding stopped, no significant difference was seen in the I_{corr} values between saline, DMEM and 25% FBS + DMEM. However, the three electrolytes' I_{corr} values were still significantly higher than the 25% FBS + PBS result at the static post-sliding condition.

These trends obviously reflected the charge transfer results, as well as wear-enhanced corrosion calculated. The charge transfer over 2-h tribocorrosion test in saline were significantly the highest than all organic-containing electrolytes, reaching $(109.01 \pm 22.49) \times 10^3$ C. The charge transfer from DMEM samples were found to be statistically below the saline values, yet higher compared to both 25% FBS-containing electrolytes. This order aligned with the wear-enhanced corrosion loss results. However, the pure corrosion loss trend was in line with the I_{corr} values obtained after 500-s post-sliding immersion. There was no significant difference in the C_0 values between saline, DMEM, and 25% FBS + DMEM, whereas the results were still statistically higher compared to the 25% FBS + PBS.

3.3 Total Volume Loss

Figure 6 compares the total volume loss (V_{total}) at the OCP condition and its conversion into specific wear rate (SWR) on CoCrMo after 2 h of tribocorrosion testing in all electrolytes, as previously reported. The V_{total} in saline electrolyte $(6.77 \pm 0.91) \times 10^6$ μm^3 was the highest after 2 h of sliding

Table 2 The average I_{corr} values calculated from the LPR measurements during tribocorrosion tests

| Conditions	Time (Second)	Current density (I_{corr}), μA.cm^{-2}			
		Saline	25% FBS + PBS	DMEM	25% FBS + DMEM
Static pre-sliding	500	0.39 ± 0.02	0.16 ± 0.06	0.30 ± 0.04	0.23 ± 0.01
Sliding	2,380	4.37 ± 0.99	0.94 ± 0.56	2.39 ± 0.54	1.17 ± 0.33
	4,260	4.42 ± 0.93	0.94 ± 0.46	2.01 ± 0.33	1.33 ± 0.13
	6,140	4.16 ± 0.98	1.00 ± 0.48	2.07 ± 1.48	1.29 ± 0.39
	8,020	4.22 ± 0.59	1.07 ± 0.52	2.02 ± 1.05	1.33 ± 0.36
Static post-sliding	8,600	0.26 ± 0.02	0.18 ± 0.05	0.25 ± 0.10	0.26 ± 0.06
Integration by Eq. (2)					
Charge transfer ($\times 10^3$ Coulomb)		109.01 ± 22.49	25.20 ± 11.17	54.70 ± 10.13	32.96 ± 7.65
Calculation by Eq. (4)					
C_0 ($\times 10^6$ μm^3)		0.30 ± 0.05	0.16 ± 0.06	0.26 ± 0.01	0.23 ± 0.03
ΔC_w ($\times 10^6$ μm^3)		3.12 ± 0.31	0.63 ± 0.15	1.46 ± 0.31	0.81 ± 0.21
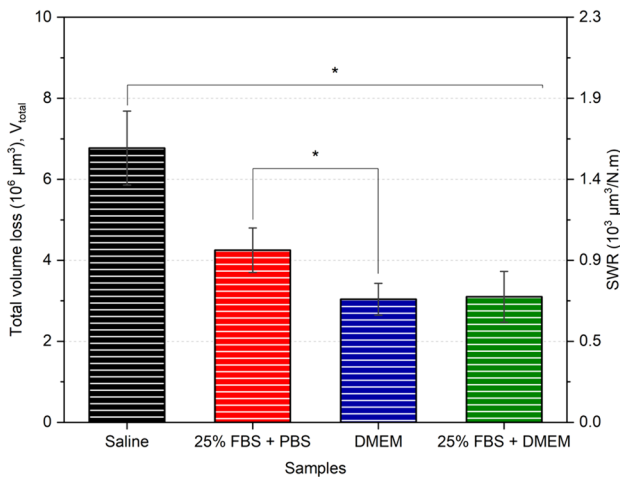
Fig. 6 Total volume loss (V_{total}) and SWR of the wear scar on CoCrMo in all electrolytes over the 2-h tribocorrosion tests at OCP ($n = 3$; SD bar; $*p < 0.05$)
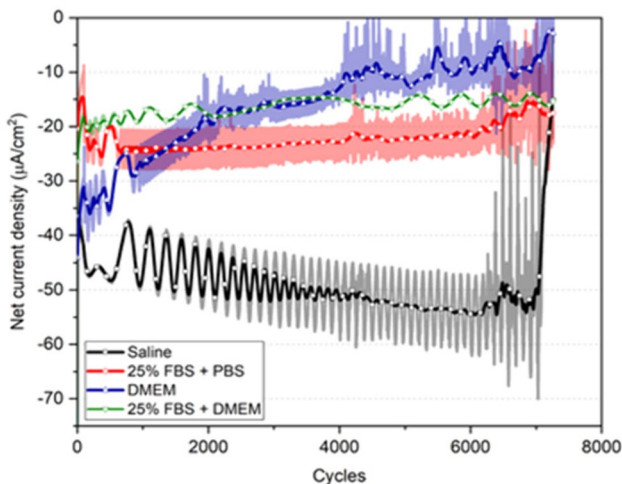

Fig. 7 Transient net current during 2-h sliding tests at a potentiostatic $E = -0.8$ V (cathodically protected) condition in all electrolytes

compared to the organic-containing electrolytes. A gradual increase in V_{total} was observed in 25% FBS + PBS compared to the DMEM sample, while no significant difference was found between V_{total} in samples tested with 25% FBS + PBS and 25% FBS + DMEM. These V_{total} values will later be split into the four components of volume loss to observe tribocorrosive degradation behavior in each electrolyte as explained earlier.

3.4 Cathodic Potentiostatic

Figure 7 illustrates the evolution of the transient net current during the 2-h sliding at $E = -0.8$ V (vs. RE Ag/AgCl) potentiostatic condition, where negative values indicate the

cathodically protected state. The current data shown is as evidence that the electrochemical degradation from corrosion on the CoCrMo surface can be disregarded. Therefore, the material loss obtained is solely due to mechanical wear degradation. The volume losses obtained by VSI on the CoCrMo at $E = -0.8$ $V_{\text{Ag/AgCl}}$ (pure wear volume loss or W_0) after 2 h of sliding in all electrolytes are presented in Fig. 8.

3.5 Material Loss Mechanisms

The V_{total} values were subtracted by the obtained values of C_0, W_0 and ΔC_W to estimate ΔW_C values in various electrolytes, compiled in Fig. 8. Table 3 presents the obtained tribocorrosion contributors based on the synergistic approach (C_0, W_0, ΔC_W and ΔW_C), while the mechanistic components (V_C and V_W) are included to complement the analysis. It shows that the W_0 in saline electrolyte was significantly higher than in the organic-containing electrolytes. No significant difference in W_0 was observed between the 25% FBS + PBS, DMEM and 25% FBS + DMEM samples during the 2-h sliding. The C_0 was significantly lower than the other volume loss contributors in all electrolytes, and no significant difference was observed in the C_0 between the samples in all electrolytes.

The CoCrMo tested in 25% FBS + PBS had the highest ΔW_C, while the DMEM had the lowest when compared to the remaining electrolytes. The ΔW_C in saline electrolyte was higher compared to 25% FBS + DMEM after the 2-h sliding tests, but it was not statistically different. However, the 25% FBS + DMEM significantly reduced the ΔW_C compared to the sample tested in 25% FBS + PBS, indicating an effect of DMEM content. On the other hand, the 25% FBS + PBS and 25% FBS + DMEM significantly reduced the ΔC_W when compared to the DMEM. The CoCrMo in saline electrolyte had the highest volume loss of ΔC_W compared to the samples tested in organic-containing electrolytes. These trends suggest that the protein content in the FBS electrolyte tends to increase the corrosion-enhanced wear loss ΔW_C but can reduce the wear-enhanced corrosion loss ΔC_W contributor during tribocorrosion on the CoCrMo surface when compared to the protein-free electrolytes (saline electrolyte and DMEM, in this case).

In Fig. 9, the contributing ratio (%) of each degradation component from their V_{total} is shown. In the saline electrolyte and DMEM, the total volume loss was mainly dominated by ΔC_W accounting for approximately ~45%, followed by W_0 at ~35%. Additionally, C_0 and ΔW_C contributed to less than ~15% each in the saline electrolyte and DMEM. Conversely, a different behavior was observed in the protein-containing electrolytes. In the 25% FBS + PBS, the total volume loss was mainly dominated by ΔC_W at ~48%, followed by W_0 at ~36%, ΔC_W and C_0. For the CoCrMo tested in 25% FBS + DMEM, the

Fig. 8 Compilation of the volume loss components when using the synergistic approach over the 2-h tribocorrosion tests (*n* = 3; SD bar; *p* < 0.05)
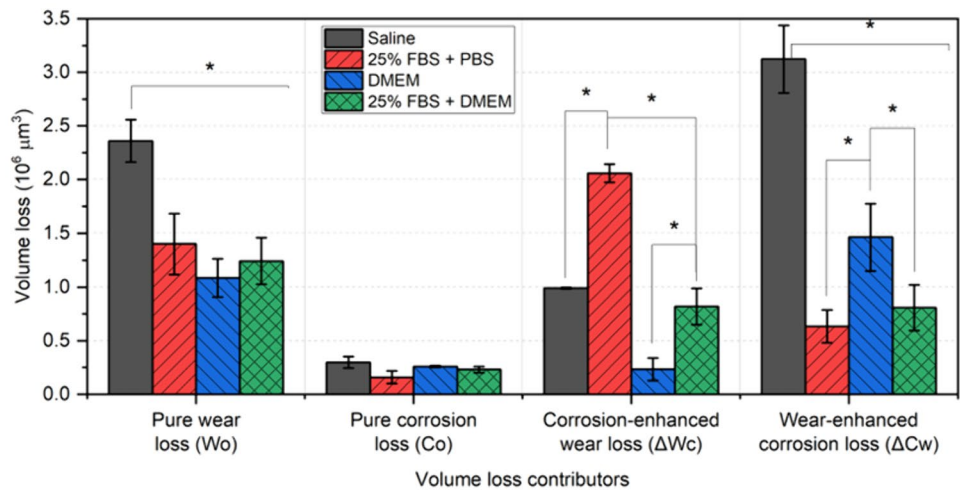

Table 3 The volumetric losses attributed to each contributor, employing both synergistic and mechanistic approaches during the 2-h tribocorrosion tests (*n* = 3; ± SD)

Electrolytes	Volume losses contributors ($\times 10^6\ \mu m^3$)						
	V_{total}	Synergistic				Mechanistic	
		C_0	W_0	ΔC_W	ΔW_C	V_C	V_W
Saline	6.77 ± 0.91	0.30 ± 0.05	2.36 ± 0.20	3.12 ± 0.31	0.99 ± 0.04	3.42 ± 0.71	3.35 ± 0.23
25% FBS + PBS	4.25 ± 0.55	0.16 ± 0.06	1.40 ± 0.28	0.63 ± 0.15	2.06 ± 0.11	0.79 ± 0.35	3.46 ± 0.23
DMEM	3.04 ± 0.39	0.26 ± 0.01	1.09 ± 0.18	1.46 ± 0.31	0.23 ± 0.14	1.72 ± 0.32	1.32 ± 0.10
25% FBS + DMEM	3.10 ± 0.63	0.23 ± 0.03	1.24 ± 0.22	0.81 ± 0.21	0.82 ± 0.20	1.04 ± 0.24	2.06 ± 0.42

Fig. 9 Ratio of each component using the synergistic approach over the 2-h tribocorrosion tests
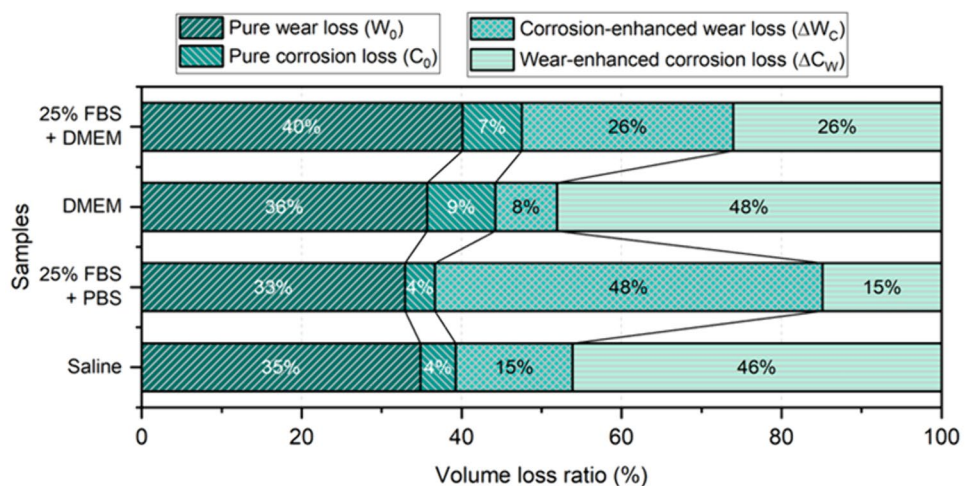
contributions of ΔW_C and ΔC_W were similar, each accounting for ~ 26% of the V_{total}. As a result, the total volume loss in the 25% FBS + DMEM was mainly dominated by W_0 at ~ 40%, while the contribution of C_0 was only ~ 4%.

3.6 SEM Imaging

Figure 10 displays SEM images of the CoCrMo wear scars following the tribocorrosion tests in different electrolytes. The wear scar from the saline test exhibited a width (~ 509.73 μm) and displayed distinct traces of abrasion
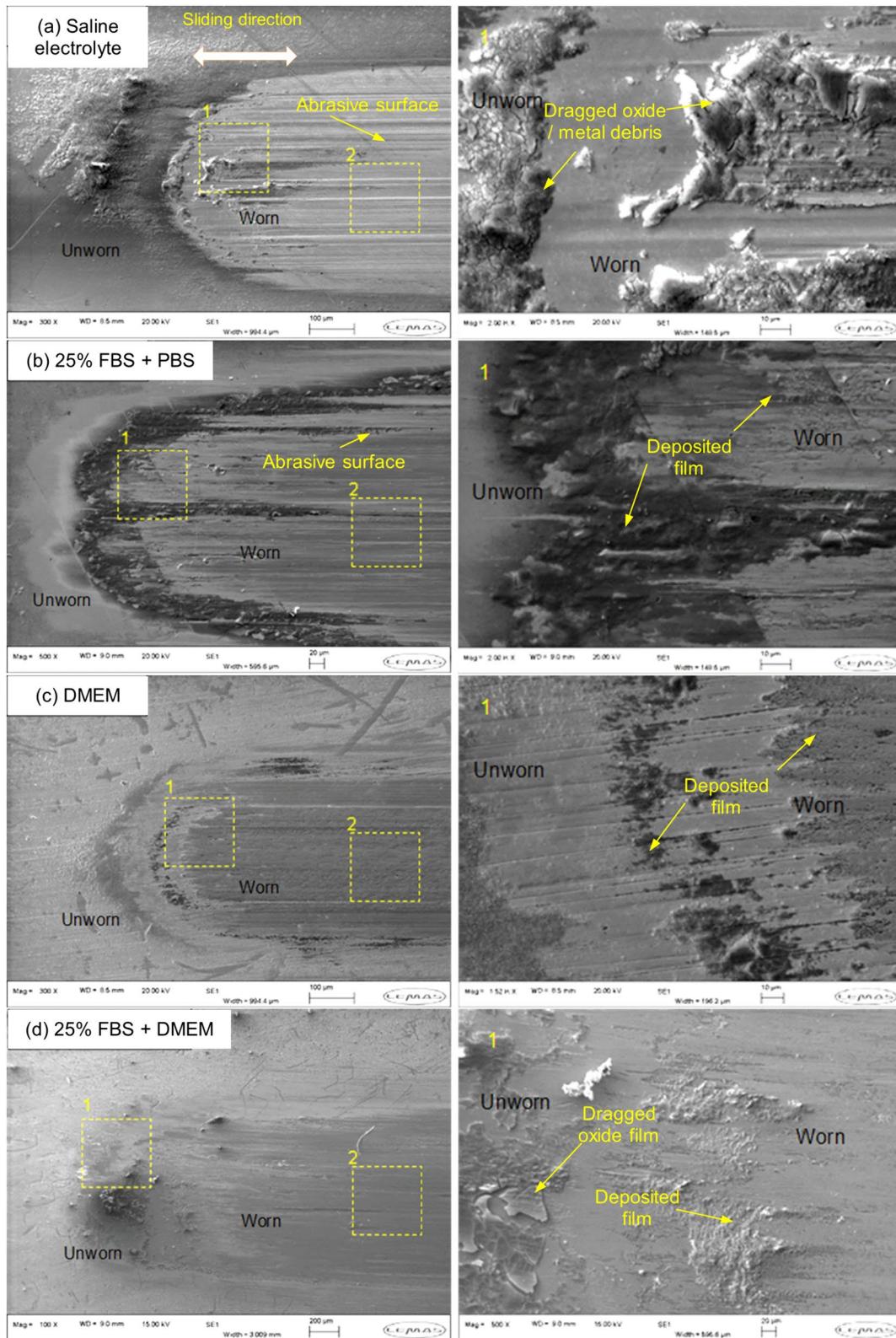
Fig. 10 SEM images of the wear tracks on CoCrMo alloy after a 2-h sliding test at OCP in **a** saline, **b** 25% FBS + PBS, **c** DMEM, and **d** 25% FBS + DMEM electrolytes

compared to the others (~ 367.67 µm for the 25% FBS-containing electrolyte). The wear track in the saline electrolyte sample showed dominating layers at the tip corner and outside, suggesting the removal and reformation of the passive film during sliding. In contrast, the wear scars in organic-containing electrolytes exhibited clear indications of layers covering the abrasive wear both on the inside and edges of scar. The chemical analysis of the tribofilm structure has been presented in the previous paper [11].

4 Discussion

This study contributes to the understanding of tribocorrosion in biomedical alloys, which is crucial for enhancing medical device performance. Building on the previous stage of the study [11], it has explored the formation of a tribofilm resulting from tribochemical reactions between simulated physiological electrolytes and cobalt alloy surfaces during sliding tests. While the previous study provided valuable insights into film composition and its impact on material loss, a comprehensive understanding of the tribocorrosion mechanism was still lacking. This study specifically focused on the role of protein in the tribocorrosive degradation of CoCrMo alloy in different simulated physiological electrolytes using both synergistic and mechanistic approaches. The tribocorrosion tests involved reciprocating ceramic ball against CoCrMo samples immersed in saline and culture medium, compared to when both electrolytes diluted with 25% fetal bovine serum (FBS). The major findings from this study reveal that protein exhibits contradictory effects on electrochemical corrosive and mechanical wear mechanisms during tribocorrosion tests. On one hand, it reduces corrosive (electrochemical) surface degradation, but on the other hand, it elevates mechanical wear degradation during sliding tests compared to tests without protein. It was noted that that tribocorrosion cannot be simplified to the addition of wear and corrosion losses, given its simultaneous mechanical and chemical events [9, 13–15], thus further discussion through tribocorrosion modes illuminated the role of protein in degradation.

4.1 Tribocorrosive Degradation Modes

To evaluate the interaction categories of mechanical wear and electrochemical losses with respect to the effect of electrolytes, the tribocorrosion mappings are shown in Fig. 11 for both modes. These mappings provide a thorough understanding of the degradation mechanisms and their relative contributions under different test conditions.

In 25% FBS-containing electrolytes, V_C, particularly ΔC_W as a synergistic component, was significantly lower than in saline and DMEM. Fig. 11a shows the interaction behavior

between corrosion and wear processes ($\Delta W_C/\Delta C_W$) using the tribocorrosion synergistic approach [23] for all investigated electrolytes in this study. The results revealed a synergistic interaction ($\Delta W_c/\Delta C_w > 1$) in the 25% FBS + PBS samples, while the saline electrolyte and DMEM samples exhibited an antagonistic-synergistic interaction ($1 > \Delta W_c/\Delta C_w \geq 0.1$). Interestingly, the CoCrMo tested in 25% FBS + DMEM displayed an intermediate behavior, lying between the synergistic and antagonistic-synergistic regimes, suggesting a contrasting role between the FBS and DMEM solutions. This suggested the beneficial role of protein in both 25% FBS + PBS and 25% FBS + DMEM decreases corrosive (electrochemical) surface degradation, unlike non-protein as in saline and DMEM solutions. As summarized by Fuentes et al. [79], the concept of metal passivity explains the autonomous formation of a passive oxide layer in passive type metals, known as passivation process and acting as a natural protection against corrosion. When two articulating surfaces experience rubbing under varying loads, velocities and directions, the passive oxide layer experience disruption and removal, triggering de-passivation. This exposes fresh material at the de-passivated surface to the surrounding electrolyte, rendering it susceptible to corrosion, leading to wear-enhanced corrosion denoted as ΔC_W. Hence, the findings of this study suggest that the presence of protein has altered the exposed surface properties once the de-passivation took place, likely by suppressing the dissolution of metal ions even before the reformation of the passive film. Mathew et al. [2] confirmed the role of bovine serum protein in generating protective films against corrosion. Yang et al. [80] employed an in situ electrochemical hip joint simulator to investigate a metal-on-polyethylene (MoP) THR's behavior during long-term walking with 30-g/L protein. To note that these results might be affected if using different contact conditions during the tribocorrosion testing, such as linear tribometer or higher load given as in this study. Their findings revealed the development of two passivation films on the interface surface along with an adsorbed protein layer, originating from precipitated and aggregated proteins. These aligned with other previous studies by the authors [29, 40] when using pre-denatured protein in FBS diluted saline compared to the ones in as-received FBS with various concentration, whereas showing that tribofilm emerged from denatured proteins and wear debris. This dual-layer formation likely contributed to reduced corrosion, promoting the corrosion inhibitory capability of both layers. SEM imaging in this study confirmed their similarity, aligning with the common assumption of a denatured protein-based tribofilm [12, 29, 81], primarily composed of graphitic carbon [11, 82]. This mechanism correlates with the de- and re-passivation process during rubbing. Protein seemed to have an active role in stabilizing OCP voltage during

Fig. 11 The impact of electrolytes on the tribocorrosive behavior using both the **a** synergistic and **b** mechanistic approaches after the 2-h sliding tests ($n=3$; SD bar)

(a)

(b)
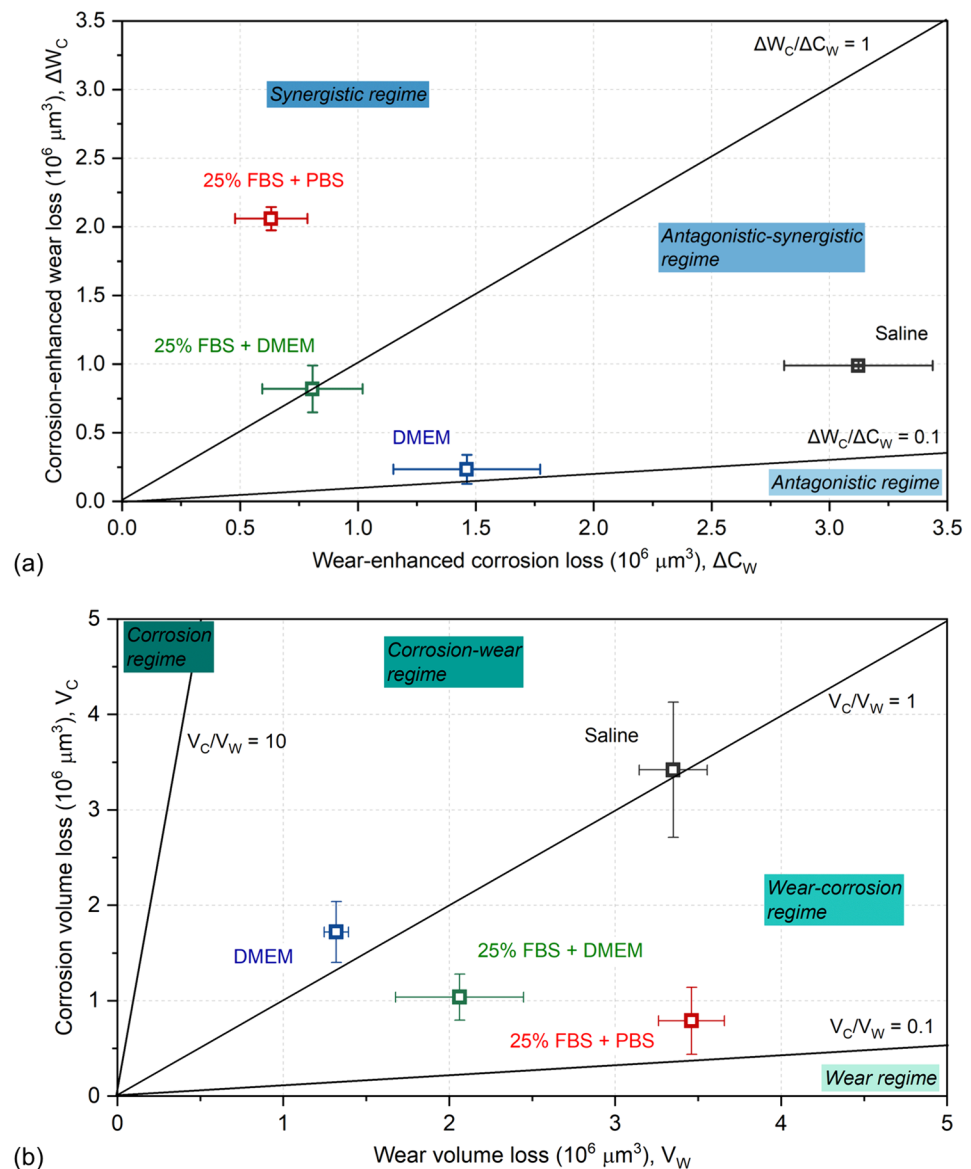
sliding, noticeable de-passivation from the initial sliding in both FBS-containing electrolytes. Although OCP trends in both electrolytes gradually dropped over the 2-h sliding, they remained higher than saline samples. The reason behind DMEM samples exhibiting the highest OCP values during sliding remains vague.

On the contrary, protein presence appeared to increase mechanical wear degradation during sliding, opposing the behavior observed in protein-free electrolytes. The influence of FBS on material degradation seemed to be primarily associated with an increase in volume loss attributed to mechanical wear (V_W). In Fig. 11b, a tribocorrosion mechanistic map [28, 78] was generated to analyze the ratios between the volume loss attributed to electrochemical corrosion (V_C) and mechanical wear (V_W). The results revealed that the tribocorrosion mechanism

in the FBS-containing electrolytes was predominantly governed by the wear-corrosion mechanism, with a ratio of $0.1 < V_C/V_W \leq 1$. This is expected to provide a deeper insight into the underlying degradation mechanisms, helping to understand the relative contributions of electrochemical corrosion and mechanical wear in different electrolytes. This is also linear with results in a synergistic context, in which this trend is confirmed by the elevated ΔW_C values observed in 25% FBS + PBS and 25% FBS + DMEM, in comparison to the saline and DMEM samples, respectively. Following the outlined process of metal passivity [79], when the freshly exposed material on the de-passivated surface comes into contact with the electrolyte, it becomes susceptible to metal ion dissolution, leading to surface roughening and concomitant corrosion-enhanced wear, referred to as ΔW_C. Simultaneously, the wear debris, comprising oxide layers,

metal ions, and detached bulk material, has the potential to undergo oxidation, binding and reactions with any present electrolyte or biological species. This aligns with the findings of the current study, suggesting that the presence of protein modifies the surface properties following the removal of the passive film, in which this alteration appears to decrease the dissolution of metal ions. However, the interaction between protein and the metal surface leads to the formation of complexes upon their removal through sliding. It has been noted in studies [79, 83] that the resulting products of metal debris-electrolyte interaction, including oxides or complex compounds, tended to accumulate and function as third bodies, escalating abrasive wear within the tribological interface, consequently increasing ΔW_C. This observation aligned with the studies conducted by Sadiq et al. [55, 84], who explored the tribocorrosion synergistic approach using CoCrMo coupled with UHMWPE in calf serum electrolyte. Their synergy mapping demonstrated that shifts between wear regimes are influenced by the interaction of proteins with the metal surface or the formation of a tribofilm. This correlation also corresponded with the increased mechanical wear attributed to protein aggregation and tribofilm presence. When comparing the transition from a non-protein to a protein-based electrolyte, it is rational to assume that protein presence indeed impacts the modification in wear behavior. Similarly, Sun et al. [85] reported that the adsorption of proteins in bovine serum onto CoCrMo alloy in a comparable testing setup reduced wear rates during sliding wear-corrosion. It suggested that the introduction of particles seemed to accelerate wear due to heightened particle entrainment. This might be also linked to particle aggregation occurring at the surface contact, consistent with the earlier findings highlighting the role of protein structure and concentration [29]. Namus et al. [54, 86] further emphasized that the worn surface of the CoCrMo alloy subjected to OCP conditions exhibited indications of mild plowing and an abrasive-corrosive wear mechanism. This observation corresponded with the SEM imaging results obtained in this study.

An investigation done by Namus et al. [86] presented an aligned trend in terms of the percentage of tribocorrosive components influenced by protein presence on CoCrMo. It observed the highest wear rate to be associated with ΔW_C, followed by W_0 and ΔC_W. This material degradation is attributed to the interplay between corrosion and mechanical response of the material under cyclic tribological loading. Alongside the comparison of different materials, the study highlighted the significant structural deterioration of the oxide layer of CoCrMo alloy under the influence of cathodic potential. Furthermore, it pointed out the synergy between corrosion and mechanical wear as the materials vulnerability, a concern particularly relevant to orthopedic environments. The specific loss of Cr ions from the oxide

film and the subsequent re-passivation process on CoCrMo hold significance in this case [41]. Nevertheless, it is worth considering that the application of cathodic protection within the synergistic method could potentially introduce result misinterpretations. This concern was acknowledged by Hesketh et al. [63], who pointed out the limitations of this approach due to the potential influence of polarization on protein adsorption [42, 54, 85]. In the broader context, the interplay between wear and corrosion, manifested through synergistic interactions, significantly contributes to the complexities of tribocorrosion and tribochemistry phenomena [87]. The occurrence of wear-corrosion dominance within the 25% FBS-containing electrolytes can be attributed to the apparent influence of protein content. While protein reduces the corrosion process, it simultaneously increases mechanical damage on the CoCrMo surface during sliding. This mechanistic behavior aligned closely with findings from Mathew et al. [2], who observed wear-corrosion as the fundamental degradation mechanism at alumina–CoCrMo interfaces within bovine calf serum electrolytes. The study elucidated that the wear-corrosion interplay could be prompted by escalating mechanical degradation due to increasing contact pressure. In contrast, the corrosion-wear mechanism predominantly occurred in saline electrolyte and DMEM. This behavior was attributed to the protein-free nature of these electrolytes, in that way elevating their role in the corrosion process.

4.2 Study Limitations

Several limitations in this study need to be acknowledged. The testing duration was limited to a 2-h sliding period, chosen for its practicality under high initial contact pressure. The previous paper [11] has reported the averaged coefficient of friction (μ) showing highest μ in saline and comparable μ in 25% FBS + PBS, DMEM, and 25% FBS + DMEM. The current study was aimed to highlight transient μ and OCP voltage trends over time. Although friction behavior during 2-h tests in protein-containing electrolytes showed no significant difference from DMEM, a longer testing duration could offer greater clarity on shifting friction behavior. Furthermore, the study employed room temperature, which was lower than bodily fluid conditions, yet the temperature of rubbing surfaces subjected to shear stress likely increased. This was not controlled in the study. Another limitation lies in the absence of testing in pure PBS, which could provide a direct comparison to protein effects via 25% FBS dilution. Additionally, measurement techniques have limitations, discussed in the previous paper [29]. LPR techniques and Stern–Geary theory suitably assess tribocorrosion currents under equilibrium conditions [88, 89]. However, sustained over-potential affects material–protein interactions and tribocorrosion mass loss mechanisms [35, 46, 53, 90, 91].

These effects are documented in prior studies and ASTM G119-09 [9, 61, 92–94]. LPR techniques assume single charge transfer reactions and a considerable distance between OCP and reversible potentials E_{rev} of anodic and cathodic reactions [95, 96]. Although the tribocorrosion system here was transient, OCP remained stable before LPR, with deviations < 3-mV/min pre-polarization. Linear E–I behavior and absence of metal deposition on counter electrode surfaces indicated separation from reversible reactions and mitigated capacitive charging effects [97, 98]. Considering the transient nature of the system and formation of surface films limiting activation-controlled corrosion reactions, variations in Tafel and proportionality constants are expected over time. While assuming a constant 120 mV/dec value, variations in β_a and β_c could introduce up to 20% maximum error in corrosion currents. Future research employing a.c. techniques will explore variations in these constants with test duration and environmental conditions.

5 Conclusion

This study successfully investigated the impact of organic species, particularly highlighted the roles of protein, in simulated physiological electrolytes on the tribocorrosive behavior of CoCrMo alloy through synergistic and mechanistic approaches. The comprehensive investigation of tribocorrosion behavior under different electrolytes led to the following key conclusions:

- The presence of protein content in the fetal bovine serum (FBS)-containing electrolytes resulted in a significant reduction in total charge transfer and volume loss due to corrosion, while simultaneously increasing the mechanical wear loss during the tribocorrosion process, as compared to the protein-free electrolytes.
- The CoCrMo sample tested in the protein-free culture medium DMEM exhibited improved mechanical wear resistance, but showed higher susceptibility to corrosion during sliding, hypothesized due to its lack of protein.
- The tribocorrosion mechanism in the protein-containing electrolytes was predominantly governed by the wear-corrosion mechanism, showing a synergistic interaction.
- In the non-protein electrolytes, such as the saline and DMEM used in this study, the tribocorrosion process was dominated by the corrosion-wear mechanism and exhibited an antagonistic-synergistic interaction.

Future studies should focus on in vivo experiments using a hip simulator to replicate real articulating joint conditions while controlling parameters. Additionally, further investigations are needed to explore the role of proteins and synovial fluid substances on surface material degradation under various joint kinematics and electrochemical conditions, involving a wider range of biomaterial alloy types. These insights are essential for optimizing biocompatibility and longevity of biomaterials in challenging biological environments affected by tribocorrosion.

Declarations

References

1. Liao, Y., et al.: CoCrMo metal-on-metal hip replacements. Phys. Chem. Chem. Phys. **15**(3), 746 (2013). https://doi.org/10.1039/c2cp42968c
2. Mathew, M.T., et al.: Tribocorrosion behavior of CoCrMo alloy for hip prosthesis as a function of loads: a comparison between two testing systems. Wear **271**(9), 1210–1219 (2011)
3. Drummond, J., Tran, P., Fary, C.: Metal-on-metal hip arthroplasty: a review of adverse reactions and patient management. J. Funct. Biomater. **6**(3), 486–499 (2015)
4. Balachandran, S., et al.: Atomic scale origin of metal ion release from hip implant taper junctions. Adv. Sci. **7**(5), 1903008 (2020)
5. Cooper, H.J., et al.: Corrosion at the head-neck taper as a cause for adverse local tissue reactions after total hip arthroplasty. J. Bone Jt. Surg. **94**(18), 1655–1661 (2012)
6. Whitehouse, M.R., et al.: Adverse local tissue reactions in metal-on-polyethylene total hip arthroplasty due to trunnion corrosion. Bone Jt. J. **97-B**(8), 1024–1030 (2015)

7. Yaszemski, M.J.: Biomaterials in Orthopedics. CRC Press, Boca Raton (2003)

8. Hill, D.: Design Engineering of Biomaterials for Medical Devices, p. 480. Wiley-VCH, Weinheim (1998)

9. López-Ortega, A., Arana, J.L., Bayón, R.: Tribocorrosion of passive materials: a review on test procedures and standards. Int. J. Corros. **2018**, 7345346 (2018)

10. Smith, A.J., et al.: Failure rates of metal-on-metal hip resurfacings: analysis of data from the National Joint Registry for England and Wales. The Lancet **380**(9855), 1759–1766 (2012)

11. Taufiqurrakhman, M., Bryant, M., Neville, A.: Tribofilms on CoCrMo alloys: Understanding the role of the lubricant. Biotribology **19**, 100104 (2019)

12. Wimmer, M.A., et al.: Wear mechanisms in metal-on-metal bearings: the importance of tribochemical reaction layers. J. Orthop. Res. **28**(4), 436–443 (2010)

13. Mathew, M.T., et al.: Significance of tribocorrosion in biomedical applications: overview and current status. Adv. Tribol. **2009**, 250986 (2009)

14. Landolt, D., Mischler, S.: Tribocorrosion of Passive Metals and Coatings. Elsevier, Amsterdam (2011)

15. Landolt, D.: Electrochemical and materials aspects of tribocorrosion systems. J. Phys. D **39**(15), 3121–3127 (2006)

16. Watson, S.W., et al.: Methods of measuring wear-corrosion synergism. Wear **181–183**, 476–484 (1995)

17. Diomidis, N., et al.: Tribocorrosion of stainless steel in sulfuric acid: identification of corrosion-wear components and effect of contact area. Wear **269**, 93–103 (2010)

18. Yan, Y.: 7—Growth of passive tribofilms in medical implants. In: Bio-tribocorrosion in Biomaterials and Medical Implants, pp. 147–168. Woodhead Publishing (2013)

19. Zhang, Y., Yin, X.-Y., Yan, F.-Y.: Tribocorrosion behaviour of type S31254 steel in seawater: identification of corrosion–wear components and effect of potential. Mater. Chem. Phys. **179**, 273–281 (2016)

20. Ma, F., et al.: Structural, mechanical and tribocorrosion behaviour in artificial seawater of CrN/AlN nano-multilayer coatings on F690 steel substrates. Appl. Surf. Sci. **428**, 404–414 (2018)

21. Priya, R., Mallika, C., Mudali, U.K.: Wear and tribocorrosion behaviour of 304L SS, Zr-702, Zircaloy-4 and Ti-grade2. Wear **310**(1), 90–100 (2014)

22. Yan, Y., Dowson, D., Neville, A.: In-situ electrochemical study of interaction of tribology and corrosion in artificial hip prosthesis simulators. J. Mech. Behav. Biomed. Mater. **18**, 191–199 (2013)

23. Stack, M.M., Abdulrahman, G.H.: Mapping erosion-corrosion of carbon steel in oil exploration conditions: some new approaches to characterizing mechanisms and synergies. Tribol. Int. **43**(7), 1268–1277 (2010)

24. Mischler, S.: Triboelectrochemical techniques and interpretation methods in tribocorrosion: a comparative evaluation. Tribol. Int. **41**(7), 573–583 (2008)

25. UNE 112086:2016: Tribocorrosion Testing Procedure for Passivating Materials. Asociación Española de Normalización (UNE) (2016)

26. Bryant, M., Neville, A.: Fretting corrosion of CoCr alloy: effect of load and displacement on the degradation mechanisms. Proc. Inst. Mech. Eng. H **231**(2), 114–126 (2017)

27. Munoz, A.I., Mischler, S.: Effect of the environment on wear ranking and corrosion of biomedical CoCrMo alloys. J. Mater. Sci. Mater. Med. **22**(3), 437–450 (2011)

28. Stack, M.M., Mathew, M.T., Hodge, C.: Micro-abrasion–corrosion interactions of Ni–Cr/WC based coatings: approaches to construction of tribo-corrosion maps for the abrasion–corrosion synergism. Electrochim. Acta **56**(24), 8249–8259 (2011)

29. Taufiqurrakhman, M., Neville, A., Bryant, M.G.: The effect of protein structure and concentration on tribocorrosion and film formation on CoCrMo alloys. J. Bio-Tribo-Corros. **7**(4), 147 (2021)

30. Uhlig, H.H.: Mechanism of fretting corrosion. J. Appl. Mech. **21**(4), 401–407 (2021)

31. Toh, W.Q., et al.: Tribochemical characterization and tribocorrosive behavior of CoCrMo alloys: a review. Materials **11**(1), 30 (2017)

32. Vinothkumar, K.R., Henderson, R.: Structures of membrane proteins. Q. Rev. Biophys. **43**(1), 65–158 (2010)

33. Bradfield, P., Dodds, J., Taylor, N.: AS Level Biology. Longman (2001)

34. Espallargas, N., et al.: In-situ generated tribomaterial in metal/metal contacts: Current understanding and future implications for implants. Biotribology **10**(Supplement C), 42–50 (2017)

35. Muñoz, A.I., Mischler, S.: Electrochemical quartz crystal microbalance and X-ray photoelectron spectroscopy study of cathodic reactions in bovine serum albumin containing solutions on a physical vapour deposition-CoCrMo biomedical alloy. Electrochim. Acta **180**(Supplement C), 96–103 (2015)

36. Muñoz, A.I., Mischler, S.: Interactive effects of albumin and phosphate ions on the corrosion of CoCrMo implant alloy. J. Electrochem. Soc. **154**(10), C562–C570 (2007)

37. Yan, Y., et al.: Real-time corrosion measurements to assess biotribocorrosion mechanisms with a hip simulator. Tribol. Int. **63**, 115–122 (2013)

38. Hesketh, J., et al.: The composition of tribofilms produced on metal-on-metal hip bearings. Biomaterials **35**(7), 2113–2119 (2014)

39. Hedberg, Y., et al.: Surface-protein interactions on different stainless steel grades: effects of protein adsorption, surface changes and metal release. J. Mater. Sci. **24**(4), 1015–1033 (2013)

40. Taufiqurrakhman, M., Neville, A., Bryant, M.: Factors influencing the bio-tribo-corrosion and chemistry on cobalt alloys: a brief literature review. AIP Conf. Proc. **2537**(1), 1 (2022)

41. Thornley, B., et al.: Investigation into the repassivation kinetics of CoCrMo for applications in a simulated biological environment. In: CORROSION 2019. 2019

42. Yan, Y., Neville, A., Dowson, D.: Biotribocorrosion of CoCrMo orthopaedic implant materials—assessing the formation and effectof the biofilm. Tribol. Int. **40**(10–12), 1492–1499 (2007)

43. Williams, D.F., Askill, I.N., Smith, R.: Protein absorption and desorption phenomena on clean metal surfaces. J. Biomed. Mater. Res. **19**(3), 313–320 (1985)

44. Ratner, B.D., et al.: Biomaterials Science: An Introduction to Materials in Medicine. Academic Press (2004)

45. Contu, F., Elsener, B., Bohni, H.: Characterization of implant materials in fetal bovine serum and sodium sulfate by electrochemical impedance spectroscopy. II. Coarsely sandblasted samples. J. Biomed. Mater. Res. A **67**(1), 246–254 (2003)

46. Kerwell, S., et al.: Electrochemically induced film formation on CoCrMo alloy for hip implant application. J. Bio Tribo Corros. (2017). https://doi.org/10.1007/s40735-016-0063-y

47. Valero-Vidal, C., et al.: Adsorption of BSA on passivated CoCrMo PVD alloy: an EQCM and XPS investigation. J. Electrochem. Soc. **161**(6), C294–C301 (2014)

48. Hedberg, Y.: Role of proteins in the degradation of relatively inert alloys inthe human body. Npj Mater. Degrad. (2018). https://doi.org/10.1038/s41529-018-0049-y

49. Arenas, M., et al.: Electrochemical noise measurements of AISI 316L during wear in simulated physiological media. Corros. Eng. Sci. Technol. **49**, 656–660 (2014)

50. Hedberg, Y.S., et al.: Can cobalt(II) and chromium(III) ions released from joint prostheses influence the friction coefficient? ACS Biomater. Sci. Eng. **1**(8), 617–620 (2015)

51. ASTM International: ASTM F75–12, in Standard Specification for Cobalt-28 Chromium-6 Molybdenum Alloy Castings and Casting Alloy for Surgical Implants (UNS R30075). ASTM International (2012)

52. Swaminathan, V., Gilbert, J.L.: Fretting corrosion of CoCrMo and Ti6Al4V interfaces. Biomaterials 33(22), 5487–5503 (2012)

53. Yoneyama, C., et al.: Influence of bovine serum albumin (BSA) on the tribocorrosion behaviour of a low carbon CoCrMo alloy in simulated body fluids. Lubricants 8(5), 61 (2020)

54. Namus, R., Rainforth, W.M.: Influence of protein adsorption on tribocorrosion behaviour of CoCrMo biomedical-grade alloys. Tribol. Int. 150, 106364 (2020)

55. Sadiq, K., Stack, M.M., Black, R.A.: Wear mapping of CoCrMo alloy in simulated bio-tribocorrosion conditions of a hip prosthesis bearing in calf serum solution. Mater. Sci. Eng. C 49, 452–462 (2015)

56. ASTM International: ASTM G5, in Standard Reference Test Method for Making Potentiodynamic Anodic Polarization Measurements. ASTM International (2014)

57. ASTM International: ASTM G59–97, in Standard Test Method for Conducting Potentiodynamic Polarization Resistance Measurements. ASTM International (2020)

58. Kestin, J., Khalifa, H.E., Correia, R.J.: Tables of the dynamic and kinematic viscosity of aqueous NaCl solutions in the temperature range 20–150 C and the pressure range 0.1–35 MPa. J. Phys. Chem. Ref. Data 10(1), 71–88 (1981)

59. Anissian, H.L., et al.: The wear pattern in metal-on-metal hip prostheses. J. Biomed. Mater. Res. 58(6), 673–678 (2001)

60. Smith, S.L., Dowson, D., Goldsmith, A.A.J.: The lubrication of metal-on-metal total hip joints: a slide down the Stribeck curve. Proc. Inst. Mech. Eng. Part J 215(5), 483–493 (2001)

61. Beadling, A.R., et al.: Tribocorrosion of hard-on-hard total hip replacements with metal and ceramic counterfaces under standard and adverse loading conditions. Tribol. Int. 103, 359–367 (2016)

62. International Organization for Standardization: ISO 14243-3:2004, in Implants for surgery—wear of total knee-joint prostheses—Part 3: loading and displacement parameters for wear-testing machines with displacement control and corresponding environmental conditions for test 2004. 2004

63. Hesketh, J., et al.: Biotribocorrosion: some electrochemical observations from an instrumented hip joint simulator. Tribol. Int. 59, 332–338 (2013)

64. Hesketh, J.E.T.: Tribocorrosion of Total Hip Replacements. University of Leeds (2012)

65. Shin, D.H., et al.: Evaluation of commercial corrosion sensors for real-time monitoring of pipe wall thickness under various operational conditions. Sensors 22(19), 7562 (2022)

66. Nazir, M.H., Saeed, A., Khan, Z.A.: Electrochemical corrosion failure analysis of large complex engineering structures by using micro-LPR sensors. Sens. Actuators B 268, 232–244 (2018)

67. Agrawal, A.K.: Corrosion monitoring. In: Buschow, K.H.J., et al. (eds.) Encyclopedia of Materials: Science and Technology, pp. 1698–1701. Elsevier, Oxford (2001)

68. Nazir, M.H., et al.: A predictive model for life assessment of automotive exhaust mufflers subject to internal corrosion failure due to exhaust gas condensation. Eng. Fail. Anal. 63, 43–60 (2016)

69. Walter, G.W.: Problems arising in the determination of accurate corrosion rates from polarization resistance measurements. Corros. Sci. 17(12), 983–993 (1977)

70. ASTM International: ASTM G119–09, in Standard Guide for Determining Synergism Between Wear and Corrosion. ASTM (2021)

71. Beadling, A.R.: Biotribocorrosion of Hard-on-Hard Bearing Surfaces in Orthopaedic Hip Replacements. University of Leeds (2016)

72. Oladokun, A.: Mechanism of Fretting Corrosion at the Modular Taper Interface of Hip Prosthesis. University of Leeds (2017)

73. Bryant, M.: Fretting-Crevice Corrosion of Cemented Metal on Metal Total Hip Replacements. University of Leeds (2013)

74. Sinnett-Jones, P.E., Wharton, J.A., Wood, R.J.K.: Micro-abrasion–corrosion of a CoCrMo alloy in simulated artificial hip joint environments. Wear 259(7), 898–909 (2005)

75. Hutchings, I., Shipway, P.: Tribology: Friction and Wear of Engineering Materials, 2nd edn., pp. 1–388. Elsevier (2017)

76. Archard, J.F.: Contact and rubbing of flat surfaces. J. Appl. Phys. 24(8), 981–988 (1953)

77. ASTM International: ASTM G119-06, in Standard Guide for Determining Synergism Between Wear and Corrosion. ASTM International (2016)

78. Stack, M.M., et al.: Some views on the construction of bio-tribocorrosion maps for Titanium alloys in Hank's solution: particle concentration and applied loads effects. Tribol. Int. 44(12), 1827–1837 (2011)

79. Fuentes, E., et al.: Advanced surface treatments on titanium and titanium alloys focused on electrochemical and physical technologies for biomedical applications. In: Biomaterial-Supported Tissue Reconstruction or Regeneration. IntechOpen (2019)

80. Yang, S., et al.: A preliminary experimental investigation on the biotribocorrosion of a metal-on-polyethylene hip prosthesis in a hip simulator. Friction 11(6), 1094–1106 (2023)

81. Maskiewicz, V.K., et al.: Characterization of protein degradation in serum-based lubricants during simulation wear testing of metal-on-metal hip prostheses. J. Biomed. Mater. Res. B 94B(2), 429–440 (2010)

82. Liao, Y., et al.: Graphitic tribological layers in metal-on-metal hip replacements. Science 334(6063), 1687–1690 (2011)

83. Espallargas, N., Torres, C., Muñoz, A.I.: A metal ion release study of CoCrMo exposed to corrosion and tribocorrosion conditions in simulated body fluids. Wear 332(Supplement C), 669–678 (2015)

84. Sadiq, K., Black, R.A., Stack, M.M.: Bio-tribocorrosion mechanisms in orthopaedic devices: Mapping the micro-abrasion–corrosion behaviour of a simulated CoCrMo hip replacement in calf serum solution. Wear 316(1), 58–69 (2014)

85. Sun, D., Wharton, J.A., Wood, R.J.K.: Micro-abrasion mechanisms of cast CoCrMo in simulated body fluids. Wear 267(11), 1845–1855 (2009)

86. Namus, R., Rainforth, W.M.: The influence of cathodic potentials on the surface oxide layer status and tribocorrosion behaviour of Ti6Al4V and CoCrMo alloys in simulated body fluid. Biotribology 30, 100212 (2022)

87. Wimmer, M.A., et al.: The effect of contact load on CoCrMo wear and the formation and retention of tribofilms. Wear 332–333, 643–649 (2015)

88. Rodríguez, G.R., Aperador, W.: Remote monitoring technique for evaluation of corrosion on reinforced concrete structures. Non-Destr. Test. (2016). https://doi.org/10.5772/62314

89. Romano, P., et al.: Monitoring of the degradation of concrete structures in environments containing chloride ions. Constr. Build. Mater. 47, 827–832 (2013)

90. Vidal, C.V., et al.: Passivation of a CoCrMo PVD alloy with biomedical composition under simulated physiological conditions studied by EQCM and XPS. J. Electrochem. Soc. 159(5), C233–C243 (2012)

91. Wang, Z., et al.: Effect of electrochemical corrosion on the subsurface microstructure evolution of a CoCrMo alloy in albumin containing environment. Appl. Surf. Sci. 406, 319–329 (2017)

92. Jellesen, M.S., et al.: Erosion–corrosion and corrosion properties of DLC coated low temperature gas-nitrided austenitic stainless steel. Wear 267(9–10), 1709–1714 (2009)

93. Mathew, M.T., Jacobs, J.J., Wimmer, M.A.: Wear-corrosion synergism in a CoCrMo hip bearing alloy is influenced by proteins. Clin. Orthop. Relat. Res. **470**(11), 3109–3117 (2012)

94. Bryant, M., et al.: Galvanically enhanced fretting-crevice corrosion of cemented femoral stems. J. Mech. Behav. Biomed. Mater. **40**, 275–286 (2014)

95. Callow, L.M., Richardson, J.A., Dawson, J.L.: Corrosion monitoring using polarisation resistance measurements: I. Techniques and correlations. Br. Corros. J. **11**(3), 123–131 (1976)

96. Callow, L.M., Richardson, J.A., Dawson, J.L.: Corrosion monitoring using polarisation resistance measurements: II. Sources of error. Br. Corros. J. **11**(3), 132–139 (1976)

97. Zhang, X.L., et al.: Effects of scan rate on the potentiodynamic polarization curve obtained to determine the Tafel slopes and corrosion current density. Corros. Sci. **51**(3), 581–587 (2009)

98. Silverman, D.C.: Tutorial on cyclic potentiodynamic polarization technique. In: CORROSION 98. 1998